

UC Santa Cruz

UC Santa Cruz Previously Published Works

Title

Graphene oxide/metal nanocrystal multilaminates as the atomic limit for safe and selective hydrogen storage

Permalink

<https://escholarship.org/uc/item/5k2661n5>

Journal

Nature Communications, 7(1)

ISSN

2041-1723

Authors

Cho, Eun Seon

Ruminski, Anne M

Aloni, Shaul

et al.

Publication Date

2016

DOI

10.1038/ncomms10804

Peer reviewed

ARTICLE

Received 14 Oct 2015 | Accepted 21 Jan 2016 | Published 23 Feb 2016

DOI: 10.1038/ncomms10804

OPEN

Graphene oxide/metal nanocrystal multilaminates as the atomic limit for safe and selective hydrogen storage

Eun Seon Cho¹, Anne M. Ruminski¹, Shaul Aloni¹, Yi-Sheng Liu², Jinghua Guo² & Jeffrey J. Urban¹

Interest in hydrogen fuel is growing for automotive applications; however, safe, dense, solid-state hydrogen storage remains a formidable scientific challenge. Metal hydrides offer ample storage capacity and do not require cryogenics or exceedingly high pressures for operation. However, hydrides have largely been abandoned because of oxidative instability and sluggish kinetics. We report a new, environmentally stable hydrogen storage material constructed of Mg nanocrystals encapsulated by atomically thin and gas-selective reduced graphene oxide (rGO) sheets. This material, protected from oxygen and moisture by the rGO layers, exhibits exceptionally dense hydrogen storage (6.5 wt% and 0.105 kg H₂ per litre in the total composite). As rGO is atomically thin, this approach minimizes inactive mass in the composite, while also providing a kinetic enhancement to hydrogen sorption performance. These multilaminates of rGO-Mg are able to deliver exceptionally dense hydrogen storage and provide a material platform for harnessing the attributes of sensitive nanomaterials in demanding environments.

¹The Molecular Foundry, Materials Sciences Division, Lawrence Berkeley National Laboratory, 1 Cyclotron Road, Berkeley, California 94720, USA. ²The Advanced Light Source, Lawrence Berkeley National Laboratory, Berkeley, California 94720, USA. Correspondence and requests for materials should be addressed to J.J.U. (email: jjurban@lbl.gov).

The established environmental impacts resulting from fossil fuels have stimulated urgent efforts to decarbonize our fuel sources. Hydrogen is the ultimate carbon-free energy carrier—it possesses the highest energy density among chemical fuels and water is the sole combustion product. Although major car manufacturers have made commitments to hydrogen as a ‘fuel of the future’¹, hydrogen storage for FCEVs (fuel cell electric vehicles) currently relies on compressed gas tanks². These are unable to meet long-term storage targets and severely compromise on-board occupancy. Metal hydrides for solid-state hydrogen storage are one of the few materials capable of providing sufficient storage density required to meet these long-term targets. However, simultaneously meeting gravimetric, volumetric, thermodynamic and kinetic requirements has proven challenging, owing to the strong binding enthalpies for the metal hydride bonds, long diffusion path lengths and oxidative instability of zero-valent metals. Although nanostructuring has been shown to optimize binding enthalpies³, synthesis and oxidative stabilization of metallic nanocrystals remains a challenge⁴. Protection strategies against oxidation and sintering of nanocrystals often involve embedding these crystals in dense matrices, which add considerable ‘dead’ mass to the composite, in turn decreasing gravimetric and volumetric density. Thus, although metal hydrides show the most promise for non-cryogenic applications, it remains true that no single material has met all of these essential criteria^{5,6}.

Here we demonstrate mixed dimensional reduced graphene oxide (GO)/Mg nanocrystal hybrids as a novel high-performance materials platform for solid-state hydrogen storage. After the first report of the preparation of individual graphene sheets in 2004 (refs 7,8), its unique optoelectronic properties attracted great attention. GO, formerly considered just a precursor for the synthesis of graphene, has begun to find independent applications in water purification and gas separations due to its hydrophilicity, chemical structure and atomistic pore size diameters^{9,10}. For example, GO membranes have recently been explored as materials for crucial gas separation challenges. Interestingly, these studies have shown extreme permeability for H₂ relative to other atmospheric gases such as O₂ and N₂, thus providing a potential avenue for use as an atomically thin, selective barrier layer for sensitive hydrogen storage materials. Furthermore, related studies have shown that reduction of GO to form reduced GO (rGO) further results in a dramatic decrease in water permeance, while maintaining desirable gas permeability characteristics¹¹. In this study, we have prepared mixed dimensional laminates of two-dimensional (2D) rGO filled with Mg nanocrystals for hydrogen storage applications (Fig. 1a). In this composite, rGO serves as the atomic limit for barrier layer materials in functional composites, providing maximum environmental protection for the least possible amount of inactive mass—theoretically, for single sheet rGO protection, up to 98 wt% of the composite mass can be active Mg—thus, this rGO composite approach yields the greatest performance in selective hydrogen permeability and kinetic enhancement in hydrogen storage. As illustrated in Fig. 1a, rGO sheets function as a protective layer against Mg nanocrystal oxidation by preventing the permeation of O₂ and H₂O, while still allowing hydrogen to easily penetrate, diffuse along the layers and be released. Moreover, beyond the crucial gas barrier behaviour, we demonstrate that the rGO layers add functionality to the laminates by reducing the activation energies associated with hydrogen absorption and desorption, key kinetically limiting steps for traditional metal hydride systems. Several studies have shown that carbon-based materials such as carbon fibres, nanotubes and graphite exhibit a beneficial catalytic effect on the kinetics and cyclability of hydrogen absorption and

desorption of metal hydrides^{12–14}. Although there are other reports using graphitic materials in composites for Li-ion battery applications, to our knowledge there have been no reports that take advantage of both the unique catalytic properties and high variability in gas permeability of rGO to synergistically yield new functionality. For the nanolaminate system presented, rGO layers are ideal encapsulating materials: they provide atomically thin structure to minimize added mass, catalytically enhanced rate-limiting hydrogen absorption/desorption events and protective barriers to prevent degradation of Mg nanocrystals.

Results

Synthesis and characterization of rGO-Mg multilaminates. The majority of reported composites consisting of metals and carbon materials are prepared via ball milling or solidification with either polymers or carbon frameworks. However, ball-milled materials are notoriously polydisperse, which introduces corresponding inhomogeneity in properties. Moreover, such energy-intensive processes can intrinsically introduce unwanted morphological disruptions and chemical inhomogeneities, all of which detract from performance. By contrast, we have developed a direct, one-pot co-reduction, thus simultaneously forming both pristine, monodisperse nanocrystals and the desired rGO without energy-intensive processing or ligand chemistries. Observing that current approaches for reduction of GO and reduction of metal precursors to form Mg nanocrystals both rely on similar methodologies^{4,15–17}, we synthesized rGO-Mg nanocomposites via a facile solution-based co-reduction method. In this process, the Mg²⁺ precursor is stabilized by GO and both of them are reduced by lithium naphthalenide. The obtained rGO-Mg was characterized via transmission electron microscopy (TEM) and X-ray diffraction (XRD), as shown in Fig. 1b,c. Mg nanocrystals were 3.26 nm diameter (± 0.87 nm) based on TEM images (Supplementary Figs 1 and 2), presenting fine monodisperse nanocrystals, compared with other metal hydrides prepared by conventional method such as ball milling. Although Scherrer analysis of the XRD peak width indicates larger crystallite size of ~ 15 nm (Supplementary Table 1), hundreds of TEM images over dozens of samples consistently show 3.26-nm-sized Mg nanocrystals. The observation of individual nanocrystals in TEM was challenging due to the low electron density of Mg, although in our materials Mg nanocrystals of diameter 3–4 nm are present and confirmed by multiple characterization methods. However, it is probable that there exist some clusters and networks of Mg particles in the sample as the XRD results imply the possible existence of a minor fraction comprising agglomerations of nanocrystals; as we discuss later, the H₂ storage properties are most consistent with \sim few nanometre-sized crystallites. The area of the peaks in electron energy loss spectroscopy (EELS) measurements (Mg \gg C > O) indicated a high density of Mg within the composite (Fig. 1d). In addition, despite containing a highly dense packing of Mg nanocrystals, the nanolaminates were observed to be remarkably environmentally stable. To investigate the limits of stability, rGO-Mg samples were exposed to air and characterized over time by XRD and TEM (Fig. 1c and Supplementary Fig. 1); remarkably, even after 3 months of air exposure, the nanocrystals remained almost entirely zero-valent crystalline Mg, while showing invasion of only a low-intensity Mg(OH)₂ peak (Supplementary Fig. 3 and an additional corrosion test result in Supplementary Fig. 4 and Supplementary Discussion). Moreover, to show the reliability offered by this approach, we completely exposed the sample to air and then demonstrated hydrogen cycling. This is not possible with any other hydride technology with comparable storage density. Although none of the techniques used for

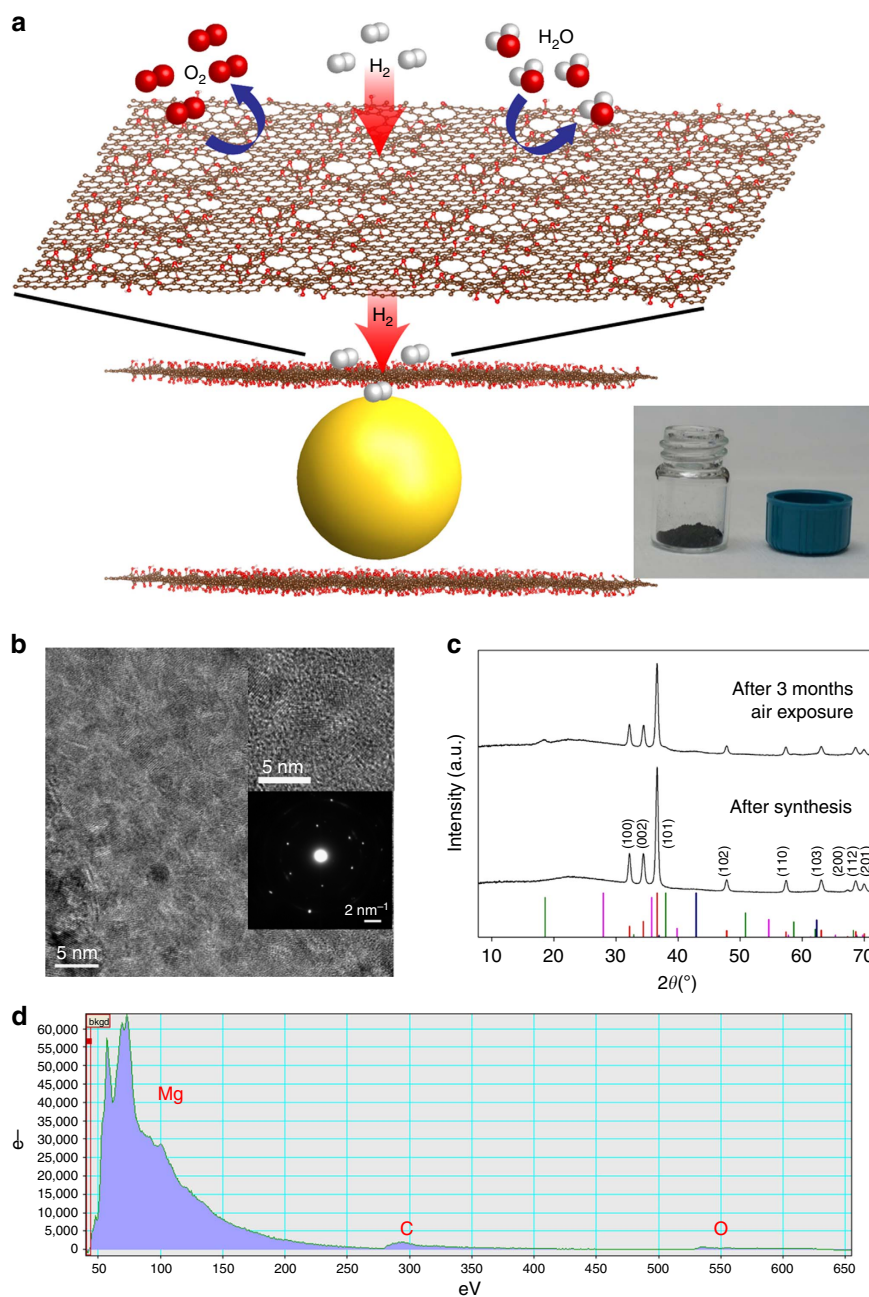


Figure 1 | Mixed dimensional rGO-Mg laminates for stable and energetically-dense hydrogen storage. (a) Illustrations depicting the structure of the rGO-Mg nanolaminates where rGO layers prevent O₂ and H₂O from penetrating, while allowing the diffusion of H₂ (inset: photograph of rGO-Mg in air). (b) TEM images of rGO-Mg showing the high density of Mg nanocrystals with no visible aggregates. The upper inset is a high-resolution image and the lower inset is diffraction pattern where the hexagonal dots are matched to Mg (100), corresponding to a *d*-spacing of 2.778 Å (JCPDS 04-0770). (More TEM images and analysis are provided in Supplementary Figs 1 and 2.) (c) XRD spectra of rGO-Mg after synthesis and after 3 months in air with indices of peaks (JCPDS 04-0770; the bottom bars represent an XRD pattern of hexagonal Mg (hcp) (red), tetragonal MgH₂ (pink), hexagonal Mg(OH)₂ (green) and cubic MgO (blue)). (d) EELS spectrum of a representative rGO-Mg composite flake suspended over a hole in the TEM support grid. The spectrum shows a dominant Mg *L*-edge peak and a carbon *K*-edge peak, indicating a large quantity of Mg crystals within the rGO support.

characterization show evidence for extensive formation of oxides of Mg (MgO or Mg(OH)₂), it is probable that a thin, self-terminating layer of oxide or sub-oxide may form on the nanocrystals; however, this oxide does not measurably have an impact on performance (Fig. 1d and Supplementary Fig. 5).

Hydrogen capacity and kinetic analysis. Hydrogen absorption and desorption characteristics of the rGO-Mg composite were tested using a Sieverts PCT-Pro instrument at 15 bar H₂ and

0 bar, respectively, as shown in Fig. 2a. Hydrogen uptake was immediate and the formation of MgH₂ was confirmed by XRD (Fig. 2c) and electron diffraction (Supplementary Fig. 1). The hydrogen absorption capacity of the composite was 6.5 wt% and 0.105 kg H₂ per litre in the total composite, which is the highest capacity reported (calculated on a full composite mass basis) using metal hydrides under the comparable conditions. This corresponds to 7.56 wt% H₂ in Mg nanocrystals, which is 99.5% of the theoretical value (7.6 wt%)⁵. Given the atomically thin

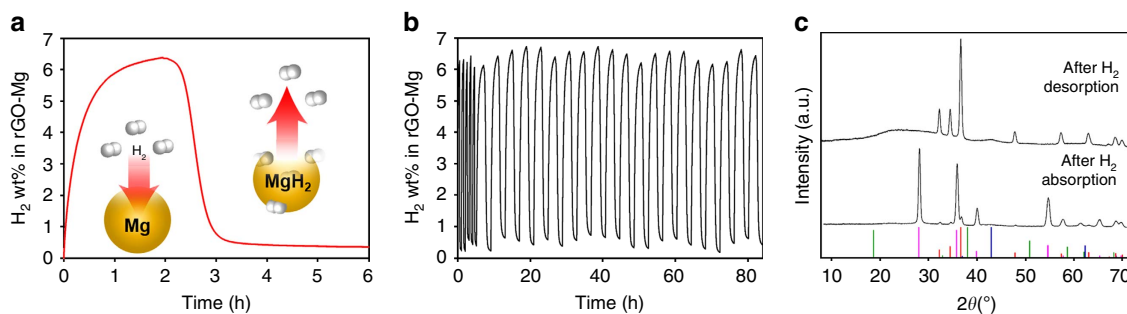


Figure 2 | Hydrogen absorption/desorption characterization of rGO-Mg multilaminates. (a) Hydrogen absorption/desorption (at 200 °C and 15 bar H_2 /300 °C and 0 bar) for the prepared rGO-Mg multilaminates. (b) Hydrogen absorption/desorption cycling of rGO-Mg multilaminates that were first exposed to air overnight. The first 5 cycles were performed at 250 °C and 15 bar H_2 /350 °C and 0 bar, and the additional 20 cycles at 200 °C and 15 bar H_2 /300 °C and 0 bar. (c) XRD spectra of rGO-Mg after absorption/desorption (the bottom bars represent the XRD patterns of Mg (red), MgH_2 (pink), $Mg(OH)_2$ (green) and MgO (blue)).

nature of the encapsulation, these nanocomposites achieve denser packing of metal nanocrystals than is possible by any competing approach, leading to optimized storage density. Furthermore, hydrogen also readily desorbed up to 6.12 wt% in the composite, thus demonstrating excellent reversibility. To verify that the hydrogen absorption was not caused by the presence of GO in the composite, control studies using only GO were conducted and exhibited minimal (<0.2 wt% in GO) absorption at 200 °C and 250 °C (Supplementary Fig. 6). This is a negligible contribution, given that the amount of GO in the multilaminates is <2 wt% overall. To analyse the kinetics, the activation energy (E_a) for hydrogen absorption/desorption was determined from measurements at three different temperatures, fitting the result with the Johnson–Mehl–Avrami model (details are described in Supplementary Discussion, Supplementary Figs 7 and 8, and Supplementary Table 2)¹⁸. The E_a values were 60.8 and 92.9 kJ mol⁻¹ for absorption and desorption, respectively, consistent with one-dimensional nucleation and growth as shown previously^{4,19}. Remarkably, these kinetics are comparable to transition metal-catalysed bulk metal-hydride systems, and the overall capacity and kinetics greatly surpass the best environmentally robust samples made up to date^{4,17}. We ascribe the performance of our composite to the unique features of this multilaminate: the nanoscale size of the Mg crystals is comparable to molecular diffusion lengths, which enables near-complete conversion to the metal hydride (99.5% of the theoretical value) and the interaction of the Mg nanocrystals with the rGO layers protects against invasion of oxygen, while enabling rapid surface diffusion of hydrogen, which enhances kinetics²⁰. Indeed, rGO-Mg hydrogen absorption/desorption is faster than Mg-polymer composites containing nanocrystals of similar size (Supplementary Fig. 9 and Supplementary Discussion). Consistent with previous studies, the diffusion of hydrogen atoms was facilitated by the interaction between Mg and carbon layers, enhancing both the hydrogen capacity and kinetics of Mg (additional data in Supplementary Fig. 10 and Supplementary Discussion)^{21,22}. Cycle tests were performed at 250 °C/350 °C for 5 cycles and at 200 °C/300 °C for additional 20 cycles (Fig. 2b). Importantly, each cycle test was conducted successively to better mimic real-world fueling/re-fueling conditions without manual evacuation in between each cycle (additional experimental results in Supplementary Fig. 11). The capacity and kinetics were well preserved during further cycles, although a slight decrease in the capacity was observed. Noticeably, the Mg nanocrystal size and size distributions were well preserved after several absorption/desorption cycles without sintering or grain growth (Supplementary Fig. 1). Although bulk metal hydrides are

susceptible to mechanical fracture and cracking due to the large volume expansion on hydriding (*ca.* 33% from Mg to MgH_2), the high Young's modulus of rGO enables it to robustly encase the Mg nanocrystals during expansion/contraction events without fracture and prevent macroscale sintering.

Structural analysis of rGO-Mg composite. X-ray absorption near-edge structure (XANES) measurements were performed to probe the interactions between rGO and Mg nanocrystals (Fig. 3a). Compared with GO, increased intensity of carbon *K*-edge at 288.4 and 290.3 eV were observed, corresponding to carbon atoms attached to oxygen or other oxygen-containing chemical species. From this, we infer that the multilaminates are uniquely stabilized by the formation of interfacial Mg–O–C bonds forged during synthesis²³. We believe this to be the basis of the exceptional stability of these multilaminates. In addition, the zero-valent state of Mg nanocrystals was verified at Mg *L*-edge measurement as both total electron yield and total fluorescence yield scans display an explicit Mg metal peak (49.8 eV) without distinct MgO peaks (Fig. 3b and additional analysis in Supplementary Fig. 5 and Supplementary Discussion), consistent with XRD and EELS spectra. The structural evolution of GO during synthesis and hydrogen cycling was studied using Raman spectroscopy (Fig. 3c,d). The intensity ratio of *D* and *G* peaks ($I(D)/I(G)$) increased after rGO-Mg synthesis, indicating that the average domain size of sp^2 hybridized regions was decreased as GO was reduced²⁴. The 2D peak, whose position and shape depends on the number of graphene layers, shifted to lower frequency (2,701 cm⁻¹ to 2,685 cm⁻¹) and its full width at half maximum also decreased on the formation of rGO-Mg (Fig. 3d). This suggests that few, if any, isolated multilayers of rGO exist in the composite, and that most rGO layers are actively wrapping Mg nanocrystals^{25,26} (additional analysis in Supplementary Fig. 12 and Supplementary Discussion). No change was observed in the Raman spectra of freshly synthesized rGO-Mg in comparison with samples studied after hydrogen cycling. Importantly, $I(D)/I(G)$ ratios remained consistent as well (1.370 after synthesis and 1.337 after cycling), indicating that the defect density, a key attribute of rGO responsible for selective hydrogen transport, was well maintained even after several hydrogen absorption and desorption cycles²⁵. In addition, the chemical environment of GO and rGO-Mg were investigated via X-ray photoelectron spectroscopy (Fig. 4). Peaks associated with oxygen-containing functional groups in the GO diminished after the formation of rGO-Mg, confirming reduction of GO²⁷. The rGO-Mg composite contained an additional peak at 282.5 eV, which is attributed to the interaction between carbon species and

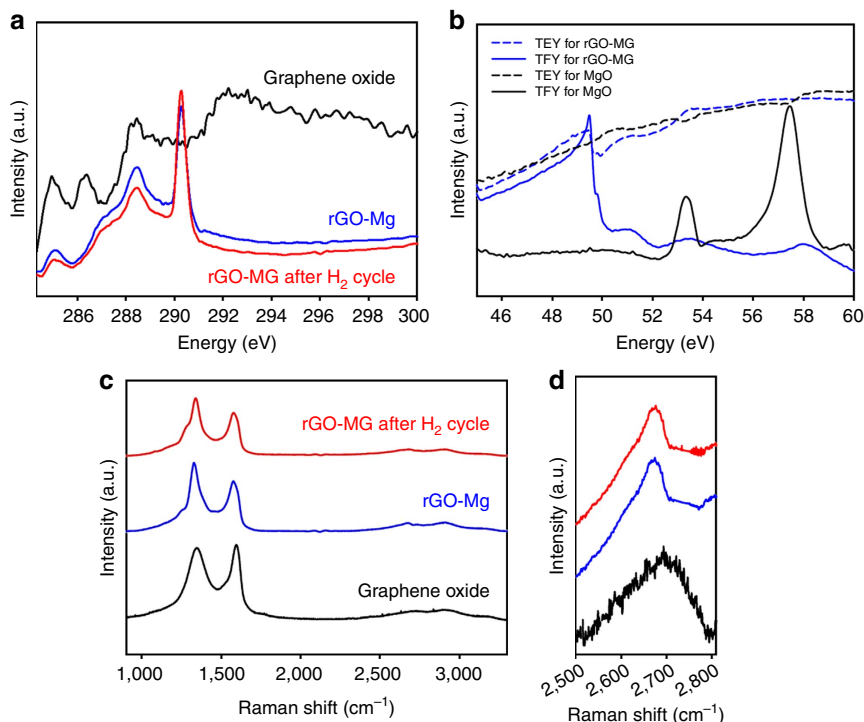


Figure 3 | XANES and Raman spectral analysis of GO and rGO-Mg multilaminates before and after hydrogen cycling. XANES spectra of (a) GO, rGO-Mg after synthesis and after cycling at carbon *K*-edge, and (b) rGO-Mg after synthesis and MgO at Mg *L*-edge. Raman spectra of (c) GO, rGO-Mg after synthesis and after H₂ cycling, and (d) the 2D peak region.

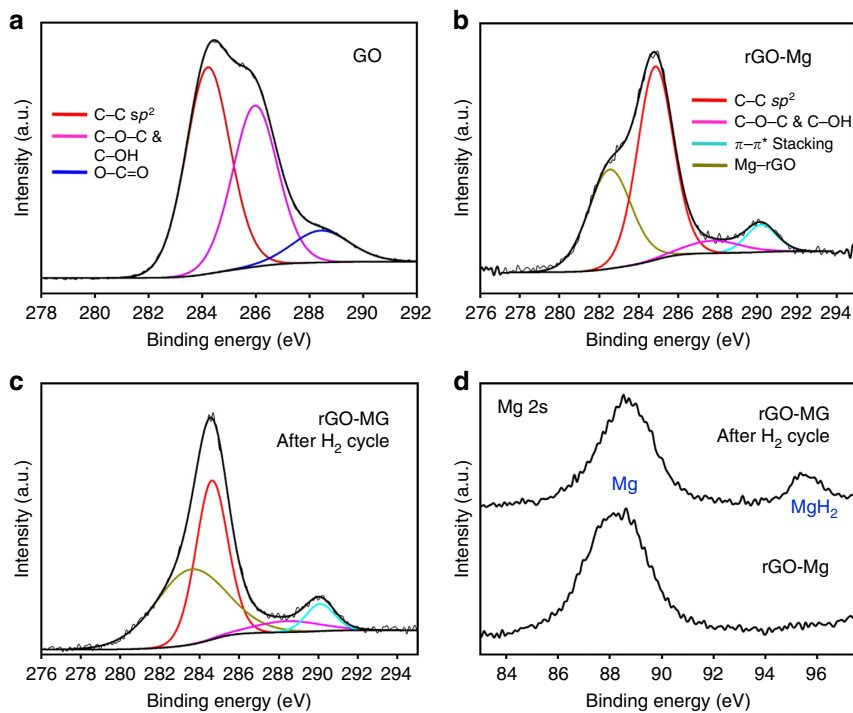


Figure 4 | X-ray photoelectron spectra (XPS) of rGO-Mg after synthesis and after hydrogen cycling. XPS spectra (C, 1s) of (a) GO, (b) rGO-Mg after synthesis and (c) rGO-Mg after H₂ cycling. (d) XPS pattern (Mg, 2s) for rGO-Mg after synthesis and after H₂ cycling.

metal particles^{28,29}, corresponding to the interaction of rGO and Mg nanocrystals. Furthermore, a prominent $\pi-\pi^*$ stacking peak was observed at 290.1 eV, resulting from Mg nanocrystal wrapping, which was also observed by TEM (Supplementary

Fig. 1). In the Mg 2s spectrum, one additional peak appears in the higher energy region after hydrogen cycling, implying a new chemical state, consistent with MgH₂ (ref. 30). The Mg and MgH₂ contents were 91.45% and 8.55%, respectively, after completing

cycle test based on Mg 2s spectrum, explaining a slight amount of the remaining hydride phase in the end of cycling.

Discussion

We have developed a facile method of preparing the densest possible loading of reactive nanocrystals safely into a composite material, a crucial step forward for enhancing the energy density of nanomaterials. As a result, our rGO-Mg multilaminates offer exceptional environmental stability and unsurpassed hydrogen storage capability, exceeding that offered by any other non-cryogenic reversible material. We believe that these results suggest the possibility of practical solid-state hydrogen storage and use in the near future. Furthermore, this work shows that atomically thin 2D materials can be used to simultaneously protect nanocrystals from ambient conditions, while also imparting new functionality. Such stable mixed dimensional laminates of zero-valent nanocrystalline metals can be extended to a variety of additional applications, including batteries, catalysis, encapsulants and energetic materials.

Methods

Synthesis of rGO-Mg nanocomposite. The composites of rGO-Mg were synthesized in an argon glove box. GO was ball milled for 10 min before use, to break it down to GO platelets so that it can effectively make a complex with bis(cyclopentadienyl) magnesium (Cp_2Mg). To prepare the lithium naphthalene solution, naphthalene (2.40 g, 0.0187 mol) was dissolved in 120 ml of tetrahydrofuran (THF), followed by the immediate addition of Li metal (0.36 g, 0.0253 mol), leading to a dark green solution. GO (6.25 mg) was dispersed in 12.5 ml of THF under Ar, sealed in a container and sonicated for 1.5 h. A Cp_2Mg solution (2.31 g, 0.015 mol, in 22.5 ml of THF) was added to GO solution afterwards, stirring for 30 min. The resulting GO/ Cp_2Mg solution was added to the lithium naphthalene solution and magnetically stirred for 2 h. The product was centrifuged (10,000 r.p.m., 20 min) and washed with THF (10,000 r.p.m., 20 min) twice, followed by vacuum drying overnight.

Characterization and instrumentation. High-resolution TEM was performed using JEOL 2100-F Field-Emission Analytical Transmission Electron operated at 120 kV and equipped with Oxford INCA energy-dispersive electron X-ray spectrometer and Tridigm Gatan imaging Filter and spectrometer. The powder samples were dispersed on lacey carbon grids from THF solutions. Elemental analysis of the EELS and energy-dispersive spectra was performed using Digital Micrograph software (Gatan Inc.). XRD patterns were acquired with a Bruker AXS D8 Discover GADDS X-Ray Diffractometer, using Cu K α radiation ($\lambda = 0.154$ nm). Hydrogen absorption/desorption measurement was performed, using a HyEnergy PCT Pro-2000 at 15/0 bar of H $_2$ at different temperatures. XANES spectroscopy was performed on Beamline 8.0.1.3 and 4.0.3 at the Advanced Light Source. The energy resolution at carbon K-edge and Mg L-edge was set to 0.1 eV and the experimental chamber had a base pressure of at most 1×10^{-8} torr. An highly ordered pyrolytic graphite (HOPG) reference sample was measured before and after all XANES experiments for energy calibration. The XANES spectra were recorded using total electron yield and total fluorescence yield detection modes. The Raman spectra of GO and rGO-Mg samples were collected using Horiba Jobin Yvon LabRAM ARAMIS automated scanning confocal Raman microscope with a 532-nm excitation source and X-ray photoelectron spectra were obtained via PHI 5400 X-ray Photoelectron Spectroscopy System with Al K α . The Mg content in the composite was determined by inductively coupled plasma-optical emission spectroscopy at the Advanced Light Source Life Sciences Division and Environmental

References

- Tollefson, J. Fuel of the future? *Nature* **464**, 1262–1264 (2010).
- Schlapbach, L. & Zuttel, A. Hydrogen-storage materials for mobile applications. *Nature* **414**, 353–358 (2001).
- Shao, H. Y., Xin, G. B., Zheng, J., Li, X. G. & Akiba, E. Nanotechnology in Mg-based materials for hydrogen storage. *Nano Energy* **1**, 590–601 (2012).
- Jeon, K. J. *et al.* Air-stable magnesium nanocomposites provide rapid and high-capacity hydrogen storage without using heavy-metal catalysts. *Nat. Mater.* **10**, 286–290 (2011).
- Aguey-Zinsou, K. F. & Ares-Fernandez, J. R. Hydrogen in magnesium: new perspectives toward functional stores. *Energy Environ. Sci.* **3**, 526–543 (2010).
- Yang, J., Sudik, A., Wolverton, C. & Siegel, D. J. High capacity hydrogen storage materials: attributes for automotive applications and techniques for materials discovery. *Chem. Soc. Rev.* **39**, 656–675 (2010).
- Novoselov, K. S. *et al.* Electric field effect in atomically thin carbon films. *Science* **306**, 666–669 (2004).

- Geim, A. K. Graphene status and prospects. *Science* **324**, 1530–1534 (2009).
- Joshi, R. K. *et al.* Precise and ultrafast molecular sieving through graphene oxide membranes. *Science* **343**, 752–754 (2014).
- Kim, H. W. *et al.* Selective gas transport through few-layered graphene and graphene oxide membranes. *Science* **342**, 91–95 (2013).
- Li, H. *et al.* Ultrathin, molecular-sieving graphene oxide membranes for selective hydrogen separation. *Science* **342**, 95–98 (2013).
- Adelhelm, P. & de Jongh, P. E. The impact of carbon materials on the hydrogen storage properties of light metal hydrides. *J. Mater. Chem.* **21**, 2417–2427 (2011).
- Yao, X. D. *et al.* Metallic and carbon nanotube-catalyzed coupling of hydrogenation in magnesium. *J. Am. Chem. Soc.* **129**, 15650–15654 (2007).
- Liu, X. F., Peaslee, D. & Majzoub, E. H. Tailoring the hydrogen storage properties of $\text{Li}_4\text{BN}_3\text{H}_{10}$ by confinement into highly ordered nanoporous carbon. *J. Mater. Chem. A* **1**, 3926–3931 (2013).
- Jung, H., Yang, S. J., Kim, T., Kang, J. H. & Park, C. R. Ultrafast room-temperature reduction of graphene oxide to graphene with excellent dispersibility by lithium naphthalene. *Carbon* **63**, 165–174 (2013).
- Rieke, R. D. Preparation of organometallic compounds from highly reactive metal powders. *Science* **246**, 1260–1264 (1989).
- Ruminski, A. M., Bardhan, R., Brand, A., Aloni, S. & Urban, J. J. Synergistic enhancement of hydrogen storage and air stability via Mg nanocrystal-polymer interfacial interactions. *Energy Environ. Sci.* **6**, 3267–3271 (2013).
- Fernandez, J. F. & Sanchez, C. R. Rate determining step in the absorption and desorption of hydrogen by magnesium. *J. Alloy Compd.* **340**, 189–198 (2002).
- Norberg, N. S., Arthur, T. S., Fredrick, S. J. & Prieto, A. L. Size-dependent hydrogen storage properties of Mg nanocrystals prepared from solution. *J. Am. Chem. Soc.* **133**, 10679–10681 (2011).
- Denis, A., Sellier, E., Aymonier, C. & Bobet, J. L. Hydrogen sorption properties of magnesium particles decorated with metallic nanoparticles as catalyst. *J. Alloy Compd.* **476**, 152–159 (2009).
- Du, A. J., Smith, S. C., Yao, X. D. & Lu, G. Q. Catalytic effects of subsurface carbon in the chemisorption of hydrogen on a Mg(0001) surface: an ab-initio study. *J. Phys. Chem. B* **110**, 1814–1819 (2006).
- Yao, X. D. *et al.* Mg-based nanocomposites with high capacity and fast kinetics for hydrogen storage. *J. Phys. Chem. B* **110**, 11697–11703 (2006).
- Wang, H. L. *et al.* An ultrafast nickel-iron battery from strongly coupled inorganic nanoparticle/nanocarbon hybrid materials. *Nat. Commun.* **3**, 917 (2012).
- Ha, H. W., Kim, I. Y., Hwang, S. J. & Ruoff, R. S. One-pot synthesis of platinum nanoparticles embedded on reduced graphene oxide for oxygen reduction in methanol fuel cells. *Electrochem. Solid State Lett.* **14**, B70–B73 (2011).
- Ferrari, A. C. & Basko, D. M. Raman spectroscopy as a versatile tool for studying the properties of graphene. *Nat. Nanotechnol.* **8**, 235–246 (2013).
- Ferrari, A. C. *et al.* Raman spectrum of graphene and graphene layers. *Phys. Rev. Lett.* **97**, 187401 (2006).
- Ganguly, A., Sharma, S., Papakonstantinou, P. & Hamilton, J. Probing the thermal deoxygenation of graphene oxide using high-resolution *in situ* X-ray-based spectroscopies. *J. Phys. Chem. C* **115**, 17009–17019 (2011).
- Jia, L. S. *et al.* Visible-light-induced photocatalyst based on C-doped LaCoO $_3$ synthesized by novel microorganism chelate method. *Catal. Commun.* **10**, 1230–1234 (2009).
- Wang, H. Q., Wu, Z. B. & Liu, Y. A simple two-step template approach for preparing carbon-doped mesoporous TiO $_2$ hollow microspheres. *J. Phys. Chem. C* **113**, 13317–13324 (2009).
- Friedrichs, O., Kolodziejczyk, L., Sanchez-Lopez, J. C., Lopez-Cartes, C. & Fernandez, A. Synthesis of nanocrystalline MgH $_2$ powder by gas-phase condensation and *in situ* hydridation: TEM, XPS and XRD study. *J. Alloy Compd.* **434**, 721–724 (2007).

Acknowledgements

Work at the Molecular Foundry and the Advanced Light Source was supported by the Office of Science, Office of Basic Energy Sciences, of the U.S. Department of Energy under Contract Number DE-AC02-05CH11231. We thank Yi-De Chuang for XANES experimental support. This material is based on work supported by the Department of Energy (DOE) through the Bay Area Photovoltaic Consortium (BAPVC) under Award Number DE-EE0004946 and also in part under the US-India Partnership to Advance Clean Energy-Research (PACE-R) for the Solar Energy Research Institute for India and the United States (SERIUS), funded jointly by the U.S. Department of Energy (Office of Science, Office of Basic Energy Sciences, and Energy Efficiency and Renewable Energy, Solar Energy Technology Program, under Subcontract DE-AC36-08GO28308 to the National Renewable Energy Laboratory, Golden, Colorado) and the Government of India, through the Department of Science and Technology under Subcontract IUSSTF/JCERDC-SERIUS/2012 dated 22 November 2012. We sincerely appreciate Jeong Yun Kim and Jayoung Kim for assisting graphic work.

Author contributions

J.J.U. and E.S.C. conceived and designed the experiments. E.S.C. synthesized and characterized the composite and performed the experiments. S.A. contributed towards TEM and EELS acquisition and analysis. Y.-S.L. and J.-H.G. performed XANES experiments. E.S.C., A.M.R. and J.J.U. analysed the data and wrote the manuscript. All authors discussed the results and commented on the manuscript.

Additional information

Supplementary Information accompanies this paper at <http://www.nature.com/naturecommunications>

Competing financial interests: The authors declare no competing financial interests.

Reprints and permission information is available online at <http://npg.nature.com/reprintsandpermissions/>

How to cite this article: Cho, E. S. *et al.* Graphene oxide/metal nanocrystal multilaminates as the atomic limit for safe and selective hydrogen storage. *Nat. Commun.* 7:10804 doi: 10.1038/ncomms10804 (2016).



This work is licensed under a Creative Commons Attribution 4.0 International License. The images or other third party material in this article are included in the article's Creative Commons license, unless indicated otherwise in the credit line; if the material is not included under the Creative Commons license, users will need to obtain permission from the license holder to reproduce the material. To view a copy of this license, visit <http://creativecommons.org/licenses/by/4.0/>